Title

Quantitative susceptibility mapping in combination with water-fat separation for simultaneous liver iron and fat fraction quantification

Authors

Lin, Huimin
Wei, Hongjiang
He, Naying
et al.

Quantitative Susceptibility Mapping in Combination with Water-Fat Separation for Simultaneous Liver Iron and Fat Fraction Quantification

Huimin Lin[1,†], **Hongjiang Wei**[2,†], **Naying He**[1], **Caixia Fu**[3], **Shu Cheng**[4], **Jun Shen**[1], **Baisong Wang**[5], **Xu Yan**[6], **Chunlei Liu**[2,7], and **Fuhua Yan**[1,*]

[1]Department of Radiology, Ruijin Hospital, Shanghai Jiao Tong University School of Medicine, Shanghai, China

[2]Department of Electrical Engineering and Computer Sciences, University of California, Berkeley, CA, USA

[3]Application development, Siemens Shenzhen Magnetic Resonance Ltd., Shenzhen, China

[4]Department of Hematology, Ruijin Hospital, Shanghai Jiao Tong University School of Medicine, Shanghai, China

[5]Department of Biological Statistics, Shanghai Jiao Tong University School of Medicine, Shanghai, China

[6]MR Collaboration NE Asia, Siemens Healthcare, Shanghai, China

[7]Helen Wills Neuroscience Institute, University of California, Berkeley, CA, USA

Abstract

[*]Corresponding Author: Fuhua Yan, Professor and Chairman of Radiology, Ruijin Hospital, Shanghai Jiao Tong University School of Medicine.NO.197 Ruijin Er Road, Shanghai China, 200025 Tel:021-64370045*665727 MP: 13661850380; yfh11655@rjh.com.cn.
[†]These authors contributed equally to this work

Purposes—To evaluate the feasibility of simultaneous quantification of liver iron concentration (LIC) and Fat Fraction (FF) using water-fat separation and quantitative susceptibility mapping (QSM).

Methods—Forty-five patients suspected of liver iron overload (LIO) were included. A volumetric interpolated breath-hold examination sequence for QSM and FF, a fat-saturated gradient echo sequence for R_2^*, a spin echo sequence for LIC measurements and MRS analyses for FF (FF-MRS) were performed. Magnetic susceptibility and FF were calculated using a water-fat separation method (FF-MRI). Correlation and Receiver operating characteristic analyses were performed.

Results—Magnetic susceptibility showed strong correlation with LIC (r_s=0.918). The optimal susceptibility cutoff values were 0.34, 0.63, 1.29, and 2.22 ppm corresponding to LIC thresholds of 1.8, 3.2, 7.0, and 15.0 mg/g dry weight. The area under the curve (AUC) were 0.948, 0.970, 1, and 1, respectively. No difference in AUC was found between susceptibility and R_2^* at all LIC thresholds. Correlation was found between FF-MRI and FF-MRS (R^2=0.910).

Conclusions—QSM has a high diagnostic performance for LIC quantification, similar to that of R_2^*. FF-MRI provides simultaneous fat quantification. Findings suggest QSM in combination with water-fat separation has potential value for evaluating LIO, especially in cases with coexisting steatosis.

Introduction

Iron overload syndrome is a common clinical problem resulting from diseases of iron hyperabsorption, as well as transfusion therapy [1]. Since no active excretion mechanism exists for excess iron of the body, iron deposes in major organs and thus may cause complications, such as liver disease and cardiomyopathy [2]. A regular monitor and clinical intervention, when necessary, are critical to prevent complications of iron overload [3]. Therefore, accurate total iron assessment is essential for the diagnosis of iron overload and for treatment monitoring to maintain relatively low iron deposits while minimizing side-effects [1].

Liver iron concentration (LIC) is considered as a reliable marker of total body iron status [1]. MRI-based R_2 and R_2^* mappings are two commonly used approaches for LIC quantification. Image-based FerriScan-R_2 (Resonance Health, Claremont, Australia) is a regulatory-approved standardized spin-echo measurement with quality-controlled iron reporting. However, high price and long scanning time narrow its widespread use [4]. Previous studies have shown that R_2^*-based MRI iron quantification approaches have strong correlations with LIC [5; 6]. However, the ability to evaluate iron level through R_2^* is influenced by the presence of fat [7]. Commonly, fat and iron coexist in patients with diffuse disease [8–11] (e.g. hereditary hemochromatosis [10] and nonalchoholic steatohepatitis [11]). The presence of fat causes additional signal modulations with echo time that lead to a

positive bias in R_2^* estimation [12]. Therefore, fat-saturation techniques were advocated by some groups [13; 14] to minimize fat signal contributions. Fat saturation could be beneficial in patients with high lipid content and relatively low iron accumulation in the liver [14]. However, it also suppresses part of the water signal, which leads to lower signal-to-noise ratio (SNR) and bias R_2^* quantification [15; 16]. In addition, coexisting steatosis in patients with iron overload is a relevant cofactor associated with the accelerated disease progression [17]. Simultaneous quantification of fat and iron overload benefits clinical management. Thus, several studies have described methods to simultaneously quantify Fat Fraction (FF) and R_2^* relaxation time in the liver [7; 11; 18–20]. In the work by Henninger *et al.* [20], a 3D-multiecho-Dixon (3D-ME-Dixon) was utilized for the simultaneous quantification. However, fat/water swaps are still problematic for Dixon techniques for patients with high LIC due to the low SNR of the original images [20].

Quantitative susceptibility mapping (QSM) is a relatively novel approach to evaluate iron deposition *in vivo* which is independent of imaging parameters. QSM utilizes the measured B_0 field to quantify the magnetic properties of tissue, such as paramagnetic compounds like iron in the cell body [21–24]. However, the application of QSM in the liver faces an additional challenge not critical in the brain - the chemical shift caused by fatty tissue. This chemical shift affects the complex-valued MRI signal, particularly the phase signal, and further QSM quantification. In this study, the confounding chemical shift was removed using a water-fat separation method [25]. Magnetic susceptibility maps were reconstructed based on the estimated B_0 field maps, and FFs were obtained from the resultant water and fat components (FF-MRI). Therefore, iron and fat level could be evaluated simultaneously from susceptibility maps and FF calculation.

The primary purpose of this study is to evaluate the diagnostic performance of QSM in liver iron quantification, with FerriScan LIC as the reference, and compare it with that of R_2^* derived from a fat-saturated multi-echo gradient echo (GRE) sequence. Furthermore, the accuracy of FF-MRI was explored by comparing with MRS-based T_2-corrected FF (FF-MRS) [26].

Methods

Patients

This prospective study was approved by the institutional review board. An informed consent was submitted by each patient. Patients suspected of liver iron overload with an elevated serum ferritin level (>500 ng/mL) were included in the study. From July 2015 to December 2016, a consecutive series of 61 (40 men, 21 women) potential study participants were approached for inclusion in this study, and 59 consented to participate. Of them, 3 patients were excluded due to claustrophobia. Data of 11 patients were unsuitable for further analysis due to obvious lesions in the right lobe of liver (n= 2) or extremely massive liver iron overload (n=9) based on MRI scans. These 9 patients with FerriScan-LIC greater than 27.5 mg/g dw showed extremely fast MRI signal decay and no reliable signal can be used for accurate field map estimation. Therefore, 45 patients with successful MRI scanning and suitable data for analysis were included in this study (Fig. 1). Demographic and clinical characteristics are shown in Table 1.

Magnetic Resonance Imaging

All MRI examinations were performed on a 1.5T scanner (MAGNETOM Aera; Siemens Healthcare, Erlangen, Germany) using a 6-channel body matrix coil and an integrated spine matrix coil. A prototype multi-echo volumetric interpolated breath-hold examination (VIBE) sequence was acquired for QSM and FF in a single breathhold of 19s, and a multi-echo 2D GRE sequence with fat saturation was performed for R_2^* in 28s with 2 breathholds (14s for each). In addition, a spin echo sequence for FerriScan-R_2 data acquisition were performed according to the manual of FerriScan centre. Table 2 lists the relevant parameters for each of the three sequences.

Magnetic Resonance Spectroscopy

The prototype MRS sequence called HISTO [26] for the reference FF estimation was scanned with the following parameters: TR=3000 ms; $TE_1\sim TE_5$=12/24/36/48/72 ms; averages=1; bandwidth=1200 Hz; vector size=1024; voxel size=12~27 cm^3; acquisition duration=15 s in one breath-hold. The volume of interest was placed on the right lobe of the liver, avoiding the main vessels and liver edges as possible.

QSM Reconstruction and FF calculation

QSM images were reconstructed using STI Suite software (https://people.eecs.berkeley.edu/~chunlei.liu/software.html). Briefly, the phase offsets between odd and even echoes are corrected prior to water-fat separation reconstruction and incorporated with a predefined fat spectrum model with 6 peaks, at [−244.3, −221.7, −175.4, −119.3, −32.1, 34.0] Hz, with relative amplitudes $0.01 \cdot [9.45e^{-i\pi0.181}, 64.66, 9.67e^{i\pi0.046}, 2.26e^{-i\pi0.567}, 2.22e^{-i\pi0.244}, 8.83e^{-i\pi0.089}]$ [25; 27]. Then, the field map is estimated using a water-fat separation method [25]. The estimated B_0 field is processed using V-SHARP to remove the background phase [28]. The filtered phase is further processed using a two-level STAR-QSM (streaking artefact reduction for QSM) algorithm [29; 30]. A schematic view of QSM reconstruction and FF calculation was shown in Fig. 2. More details can be found in the Supplementary material.

Data Analysis

VIBE and GRE datasets were analysed by two radiologists specializing in liver imaging (reader 1: HM. L with 3 years of experience, and reader 2: NY. H, with 5 years of experience). R_2^* was computed with a three-parameter curve-fitting model (offset model) [31] on a workstation (ADW 4.6, GE Healthcare). Susceptibility values and FF-MRI were measured with ImageJ software (version 1.6; National Institutes of Health, Bethesda, MD). The acquired SE MR data were subsequently uploaded to Resonance Health (http://www.resonancehealth.com/) for FerriScan- LIC assessments.

On susceptibility maps, circular regions of interest (ROIs) were drawn in the inferior slices of right hepatic lobe, avoiding vessels, borders, and artefacts. Liver susceptibility values were referenced to mean susceptibility value of the paravertebral muscle tissue by placing additional ROIs at the renal hilum level, since paravertebral muscle doesn't accumulate excess iron [21]. ROIs on susceptibility images were drawn on three consecutive slices (Fig. 3). The ROI on the R_2^* map was delineated in a visual alignment with the liver ROI of the

susceptibility map, and the ROI of FF-MRI was approximately co-localized to the MRS voxel.

The spectra data was processed using the method described in [26] to estimate the T_2-corrected FF. The integrals of water and fat signal on the real part of the spectra at each TE were automatically generated by the syngo Spectroscopy software (Siemens Healthcare). Manual adjustment in phase and baseline correction steps was executed in case that the automatic scheme failed. Subsequently, the integrals were fit to a monoexponential model using an in-house developed MATLAB (Mathworks, Natick MA) program to obtain the T_2-corrected water and fat content (S_0_fat and S_0_water). Finally, the T_2-corrected fat fraction was calculated as FF = S_0_fat / (S_0_fat + S_0_water) *100%.

Statistical Analysis

Intraclass correlation coefficients (ICC) were performed to test the inter-rater reliability between measurements (QSM, R_2^*) by two readers. An ICC of 0.8–1.00 was considered to indicate excellent agreement; 0.61–0.8, good agreement; 0.41–0.60, moderate agreement; 0.21–0.40, fair agreement; and 0.2 or less, slight agreement. If excellent agreement was obtained, the datasets were averaged for further analyses. The data were descriptively analysed and statistically tested for normality using the Shapiro-Wilk test. Spearman correlation analyses were performed to analyse the correlations between QSM and FerriScan-LIC, and between R_2^* and FerriScan-LIC. Linear regression analysis was performed to compare the FF-MRI and FF-MRS.

Five grades (normal, mild, moderate, heavy, and extremely-heavy grade) were assigned using the clinical LIC grading thresholds (1.8, 3.2, 7.0, and 15.0 mg/g dw). FerriScan-LIC was set as the reference for LIC grades. Receiver operating characteristic (ROC) analysis was performed and the area under the ROC curve (AUC) was calculated for both QSM and R_2^*. The optimal cutoff value was the value at which the sum of the sensitivity and specificity was maximized. Two paired ROC curves were compared using the method developed by DeLong *et al.* [32].

All these statistical analyses were performed using the SPSS software (SPSS version 23.0; SPSS Inc., Chicago, IL) and MedCalc software (MedCalc version 15, Mariakerke, Belgium). The statistical significance threshold was set at *P*<0.05.

Results

Susceptibility and R_2^* Assessment

All 45 patients were included for the estimation of susceptibility, R_2^*, and LIC. The mean size of the liver and muscle ROIs on the susceptibility map was 1.72±0.46 cm^2 (range, 1.04~2.59 cm^2) and 0.79±0.28 cm^2 (range, 0.39~1.23 cm^2), respectively. The ICCs for susceptibility and R_2^* between the two observers were 0.973 and 0.998, respectively. The mean value for susceptibility, R_2^* and LIC were 1.25±1.41 ppm (range, -0.23~5.94 ppm), 236.14±247.47 s^{-1} (range, 32.98~926.49 s^{-1}), and 6.70±7.43 mg/g dw (range, 0.5~27.5 mg/g dw), respectively. Shapiro-Wilk test showed a non-normal distribution for all these datasets.

Correlations between Susceptibility and FerriScan-LIC, and between R_2^* and FerriScan-LIC

With increased iron concentration confirmed by FerriScan-LIC, VIBE magnitude images showed consistent signal decay, and both R_2^* and susceptibility values were increased accordingly (Fig. 4). Positive correlations were found (Fig. 5) between susceptibility and FerriScan-LIC (r_s=0.918; 95% confidence interval [CI]: 0.855, 0.954; P<0.001), and between R_2^* and FerriScan-LIC (r_s=0.946; 95% CI: 0.903, 0.970; P<0.001).

Diagnostic Performance of Grading based on LIC levels

The optimal susceptibility cutoff values for each LIC threshold were 0.34 ppm (1.8 mg/g dw), 0.63 ppm (3.2 mg/g dw), 1.29 ppm (7.0 mg/g dw), and 2.22 ppm (15.0 mg/g dw),respectively. For R_2^*, the optimal cutoff values were 58.01, 158.86, 282.94, and 469.31 s^{-1}, respectively. The AUCs for QSM cutoff values were 0.948, 0.970, 1 and 1, while for R_2^* thresholds were 0.969, 0.972, 0.997, and 1, respectively. There was no significant difference between the AUCs for QSM and R_2^* at all the four LIC grading levels (Table 3).

FF Assessments with MRI and MRS

The fat peaks of 20 patients were difficult to be recognized from MRS, probably due to iron-related rapid signal decay (n=10, LIC ranging from 9.9 to 27.5 mg/g dw) and extremely low-fat content (n=9). Besides, 2 cases were also excluded because of both the high iron (LIC=8.8 and 21.3 mg/g dw, respectively) and extremely low-fat content. Thus, the remaining 24 patients were included in the FF analysis. The mean FF-MRI and mean FF-MRS were 8.00% (range, 2.00%~22.90%), and 5.69% (range, 0.41%~18.87%). FF-MRI showed a strong correlation with FF-MRS (R^2=0.910, P<0.01). The linear regression line (Fig. 6) between FF-MRI and FF-MRS had a slope of 1.09 (P<0.01) and an intercept of 1.91(P<0.01).

Discussion

The findings of this study demonstrated that QSM showed strong correlation with FerriScan-LIC (r_s=0.918). ROC analysis further demonstrated that QSM could grade LIC (normal to extremely-heavy grades), with high diagnostic performance similar to that of R_2^*. Furthermore, FF-MRI was strongly correlated with FF-MRS (R^2=0.910). These results suggest that QSM provides the necessary information to assess LIC, and that fat fraction can be quantified from the same single scan using a water-fat separation method.

In this study, the strong correlation (r_s= 0.918) between QSM and FerriScan-LIC was consistent with a previous study [33] (r_p=0.872 at 1.5T), indicating the role of QSM as a promising imaging biomarker for quantifying hepatic iron overload. This previous study set subcutaneous adipose tissue as the susceptibility reference [33], while we use paravertebral muscle as the susceptibility reference. High correlation coefficients for these two approaches demonstrate that either subcutaneous adipose tissue or paravertebral muscle can be used as the susceptibility reference. Some of the participants recruited in this study showed little accumulation of subcutaneous adipose tissue, which could be due to hypermetabolic conditions [34]. Limited adipose area increased the difficulty to draw the reference ROIs for

reference susceptibility value calculation. Thus, as proposed by the previous study [21], we choose paravertebral muscle as the reference.

The value of R_2^*-based MRI techniques has been approved by the American Society of Haematology [35]. Although the R_2^* bias increased with R_2^*, studies demonstrated the bias induced by the use of saturation were small and did not cause a clinically significant difference, when the measured R_2^* values were confined to a range below 500 s^{-1} [13; 15; 16]. In the current study, 6 of the 45 patients had R_2^* values above 500 s^{-1}. This could be the reason why the estimated R_2^* based on the fat-saturated GRE sequence showed good diagnostic performances, with all the AUCs greater than 0.95. ROC analyses demonstrated the high diagnostic performance of QSM to quantify LIC. Meanwhile, the diagnostic performance of QSM showed no significant difference with that of R_2^* at the LIC thresholds of 1.8, 3.2, 7.0, and 15 mg/g dw. LIC greater than 1.8 mg/g dw is considered to reach the diagnosis of iron overload. LIC greater than 3.2 mg/g dw is the clinically significant threshold for iron chelation therapy, the LIC of 7.0 mg/g dw is a key threshold for iron chelation therapy initiation and efficacy monitoring, and LIC of 15 mg/g dw is an indicator of substantial risk for cardiac diseases and early death in thalassemia [36]. Hence, QSM might be useful not only in the detection of lower levels of iron accumulation, but also in the guidance of iron chelation therapy.

Coexisted fat and iron play an interactive aggressive role in the disease progression [8; 9]. As we know, oxidative stress induced by iron accumulation within hepatocytes contributes to the end-stage cirrhosis and development of hepatocellular carcinoma in patients with hemochromatosis. Moreover, cirrhosis plays a major role for the increased risk of liver cancer [37]. Steatosis has shown to be a relevant cofactor adding to the effect of iron in accelerating fibrosis [17]. Steatosis also shows the predisposition to diabetes, which is considered as a clear risk factor for advanced hepatic fibrosis [10]. Management of cofactors is important to reduce the risk of liver fibrosis [10], consequently decreasing the risk of liver failure and liver cancer. Thus, simultaneous iron and fat quantification is imperative. Interestingly, FF-MRI from the water-fat separation method showed strong correlations with FF-MRS. Previous studies of hepatic MRS have demonstrated its value as a useful examination of lipid content [34]. Meanwhile, a previous study demonstrated that T_2-corrected FF by MRS was not correlated with the histologic degree of iron deposition [38]. However, MRS voxels are acquired in a breath-hold state according to the manual placement on its localizer images. There are still possible inconsistencies between the actual acquired voxel position and the planned position. Besides, FF-MRS reflects the FF of voxels, while FF-MRI is a ROI-based fat estimation [20]. Both of them might be the reasons for the bias between FF-MRS and FF-MRI, even though FF-MRS is accepted as a "gold standard" and visual alignment was performed as possible. Note that, water-fat separation reconstruction was conducted using a predefined fat spectrum model derived from food oil experiments [25; 27], in the present study. Different fat spectra derived from liver MRS [27], are also compatible for the water-fat separation in our study. Recently, one study by Hong *et al.* has demonstrated that there was no obvious bias for liver PDFF estimation when using different biologically plausible fat spectral models [39].

These findings demonstrated that QSM is feasible to evaluate hepatic iron, with simultaneous fat fraction estimation. Based on the water-fat separation model, we can estimate water, fat, R_2^* and B_0 field map. From these estimated components, the FF and susceptibility value are computed. The computed susceptibility values showed a strong correlation with FerriScan-LICs, which provides a new insight to quantify the iron content that coexists with fat. Although the manufacturer-provided MRS was chosen for the reference FF estimation in cases with coexisting iron by many studies [20; 40], the relative long TE_{min} (12 ms) and TE spacing was not applicable in cases with extremely high iron levels. While FF-MRI can provide an estimation of FF in these high-iron cases, the accuracy is not evaluated due to the lack of an FF-MRS reference. Nevertheless, FF-MRI showed a strong correlation with FF-MRS in lower LIC levels, which still demonstrated that water-fat separation is promising for fat quantification. This is, to our best knowledge, the first study reporting the simultaneous evaluation of iron and fat using QSM in combination with a water-fat separation method.

There are several approaches with respect to simultaneous fat and R_2^* measurements [7; 11; 18–20]. In the works of Galimberti *et al.* [18] and Franca *et al.*[19], 2D multi-echo GRE sequences were utilized to accurately quantify liver R_2^* and FF simultaneously for patients with iron overload. Henninger *et al.* [20] used a 3D-ME-Dixon for simultaneous iron and fat quantification. Iron and fat can be measured throughout the liver within a breath-hold with this sequence, while 2D GRE might need multiple breath-hold acquisitions at lower slice resolution. The 3D-ME-Dixon sequence was considered as a valuable tool for the estimation of hepatic iron and fat in a clinical setting. However, with the inline calculation used in their study, fat/water-swaps remained a drawback, and the measurable R_2^* values were constrained to 400 s^{-1} in order to avoid deviation induced by the inline fitting algorithm of that particular version [41]. Note that the highest estimated R_2^* value depends on different parameters, for example, field strengths, imaging acquisition parameters , and different fitting algorithms [42]. In the present study, QSM analyses were available for patients whose R_2^* were up to 926.49 s^{-1} using a similar 3D Dixon sequence, though QSM reconstruction needs a few steps off-line post-processing.

There were also several limitations in our study. First, we employed FerriScan-based LIC and FF-MRS as the references. On one hand, liver biopsy was not performed considering safety reasons. On the other hand, regulatory-approved FerriScan-LIC was verified as a reliable and accurate method to evaluate LIC in a multicentre validation study [43]. Although FF-MRI showed strong correlation with FF-MRI in lower LIC levels, the feasibility of FF-MRI estimation in cases with higher iron still need further studies. Second, the possible interferences of confounding factors (i.e. inflammation and fibrosis) with liver susceptibility measurements were not investigated in the present study. A previous study has shown that inflammation and fibrosis contribute diamagnetic (negative) susceptibility in kidney [44]. Interferences of inflammation and fibrosis with liver susceptibility need to be fully considered in further studies. Third, QSM was not available in the quantification of extremely massive iron overload (e.g. LIC>27.5 mg/g dw). For these patients with extremely iron overload, the signal decays faster, and phase values may be below the noise level, and phase unwrapping is challenging with low signal-to-noise ratio. Thus, B_0 field may be underestimated, which is a limitation of QSM for quantifying extremely iron overload. It

could be addressed using ultrashort TE sequences in future studies [45]. As for R_2^*, extremely rapid signal decay may also impose a limitation for accurate iron quantification, though it can be addressed by shorter echo spaces and minimum first TE [46]. Considering that the susceptibility and R_2^* are based on different contrast mechanisms, although R_2^* shows a little bit higher correlation with LIC, the R_2^* suffers from non-local susceptibility effects and still confounds its accuracy for evaluating iron content [47]. Finally, using a flip angle of 6° at a TR of 10ms in current study, may have introduced the possibility of T_1 weighting in the FF estimation. Since the signal decays faster and higher SNR is critical for accurately estimating B_0 field map in cases with high iron levels, the flip angle of 6°, also used in one previous study [48], was chosen as a tradeoff between the T1 bias and adequate SNR for B_0 field map estimation.

In conclusion, QSM in combination with water-fat separation is valuable in quantification and grading of liver iron overload, especially in cases with coexisting steatosis.

Supplementary Material

Refer to Web version on PubMed Central for supplementary material.

Acknowledgments

Abbreviations

AUC	the area under the curve
FF-MRI	FF calculated with a water-fat separation method
FF-MRS	MR Spectroscopy based FF
FF	Fat Fraction
FOV	field of view
GRE	gradient echo
ICC	Intraclass correlation coefficients
LIC	liver iron concentration
LIO	liver iron overload
mg/g dw	mg/g dry weight
QSM	Quantitative Susceptibility Mapping

| ROC	Receiver operating characteristic
ROI	region of interest
VIBE	volumetric interpolated breath-hold examination

References

1. Brittenham GM, Badman DG, National Institute of D, Digestive, Kidney Diseases W. Noninvasive measurement of iron: report of an NIDDK workshop. Blood. 2003; 101:15–19. [PubMed: 12393526]

2. Vermylen C. What is new in iron overload? Eur J Pediatr. 2008; 167:377–381. [PubMed: 17899187]

3. Chou ST, Fasano RM. Management of Patients with Sickle Cell Disease Using Transfusion Therapy: Guidelines and Complications. Hematol Oncol Clin North Am. 2016; 30:591–608. [PubMed: 27112998]

4. Wood JC. Estimating tissue iron burden: current status and future prospects. Br J Haematol. 2015; 170:15–28. [PubMed: 25765344]

5. Wood JC, Enriquez C, Ghugre N, et al. MRI R2 and R2* mapping accurately estimates hepatic iron concentration in transfusion-dependent thalassemia and sickle cell disease patients. Blood. 2005; 106:1460–1465. [PubMed: 15860670]

6. Hankins JS, McCarville MB, Loeffler RB, et al. R2* magnetic resonance imaging of the liver in patients with iron overload. Blood. 2009; 113:4853–4855. [PubMed: 19264677]

7. Kuhn JP, Hernando D, Munoz del Rio A, et al. Effect of multipeak spectral modeling of fat for liver iron and fat quantification: correlation of biopsy with MR imaging results. Radiology. 2012; 265:133–142. [PubMed: 22923718]

8. Moirand R, Mortaji AM, Loreal O, Paillard F, Brissot P, Deugnier Y. A new syndrome of liver iron overload with normal transferrin saturation. Lancet. 1997; 349:95–97. [PubMed: 8996422]

9. George DK, Goldwurm S, MacDonald GA, et al. Increased hepatic iron concentration in nonalcoholic steatohepatitis is associated with increased fibrosis. Gastroenterology. 1998; 114:311–318. [PubMed: 9453491]

10. Wood MJ, Powell LW, Dixon JL, Ramm GA. Clinical cofactors and hepatic fibrosis in hereditary hemochromatosis: the role of diabetes mellitus. Hepatology. 2012; 56:904–911. [PubMed: 22422567]

11. Kuhn JP, Meffert P, Heske C, et al. Prevalence of Fatty Liver Disease and Hepatic Iron Overload in a Northeastern German Population by Using Quantitative MR Imaging. Radiology. 2017; 284:706–716. [PubMed: 28481195]

12. Reeder SB, Sirlin CB. Quantification of liver fat with magnetic resonance imaging. Magn Reson Imaging Clin N Am. 2010; 18:337–357. ix. [PubMed: 21094444]

13. Henninger B, Zoller H, Rauch S, et al. R2* relaxometry for the quantification of hepatic iron overload: biopsy-based calibration and comparison with the literature. Rofo. 2015; 187:472–479. [PubMed: 25877992]

14. Sanches-Rocha L, Serpa B, Figueiredo E, Hamerschlak N, Baroni R. Comparison between multi-echo T2* with and without fat saturation pulse for quantification of liver iron overload. Magn Reson Imaging. 2013; 31:1704–1708. [PubMed: 23978552]

15. Krafft AJ, Loeffler RB, Song R, et al. Does fat suppression via chemically selective saturation affect R2*-MRI for transfusional iron overload assessment? A clinical evaluation at 1.5T and 3T. Magn Reson Med. 2016; 76:591–601. [PubMed: 26308155]

16. Meloni A, Tyszka JM, Pepe A, Wood JC. Effect of inversion recovery fat suppression on hepatic R2* quantitation in transfusional siderosis. AJR Am J Roentgenol. 2015; 204:625–629. [PubMed: 25714295]

17. Powell EE, Ali A, Clouston AD, et al. Steatosis is a cofactor in liver injury in hemochromatosis. Gastroenterology. 2005; 129:1937–1943. [PubMed: 16344062]

18. Galimberti S, Trombini P, Bernasconi DP, et al. Simultaneous liver iron and fat measures by magnetic resonance imaging in patients with hyperferritinemia. Scand J Gastroenterol. 2015; 50:429–438. [PubMed: 25633726]

19. Franca M, Alberich-Bayarri A, Marti-Bonmati L, et al. Accurate simultaneous quantification of liver steatosis and iron overload in diffuse liver diseases with MRI. Abdom Radiol (NY). 2017; 42:1434–1443. [PubMed: 28110367]

20. Henninger B, Zoller H, Kannengiesser S, Zhong X, Jaschke W, Kremser C. 3D Multiecho Dixon for the Evaluation of Hepatic Iron and Fat in a Clinical Setting. J Magn Reson Imaging. 2017; 46:793–800. [PubMed: 28225576]

21. Taylor BA, Loeffler RB, Song R, McCarville MB, Hankins JS, Hillenbrand CM. Simultaneous field and R2 mapping to quantify liver iron content using autoregressive moving average modeling. J Magn Reson Imaging. 2012; 35:1125–1132. [PubMed: 22180325]

22. Liu C, Wei H, Gong NJ, Cronin M, Dibb R, Decker K. Quantitative Susceptibility Mapping: Contrast Mechanisms and Clinical Applications. Tomography. 2015; 1:3–17. [PubMed: 26844301]

23. Wei H, Xie L, Dibb R, et al. Imaging whole-brain cytoarchitecture of mouse with MRI-based quantitative susceptibility mapping. Neuroimage. 2016; 137:107–115. [PubMed: 27181764]

24. Sharma SD, Fischer R, Schoennagel BP, et al. MRI-based quantitative susceptibility mapping (QSM) and R2* mapping of liver iron overload: Comparison with SQUID-based biomagnetic liver susceptometry. Magn Reson Med. 2017; 78:264–270. [PubMed: 27509836]

25. Yu H, Shimakawa A, McKenzie CA, Brodsky E, Brittain JH, Reeder SB. Multiecho water-fat separation and simultaneous R2* estimation with multifrequency fat spectrum modeling. Magn Reson Med. 2008; 60:1122–1134. [PubMed: 18956464]

26. Pineda N, Sharma P, Xu Q, Hu X, Vos M, Martin DR. Measurement of hepatic lipid: high-speed T2-corrected multiecho acquisition at 1H MR spectroscopy--a rapid and accurate technique. Radiology. 2009; 252:568–576. [PubMed: 19546430]

27. Hamilton G, Yokoo T, Bydder M, et al. In vivo characterization of the liver fat 1H MR spectrum. NMR Biomed. 2011; 24:784–790. [PubMed: 21834002]

28. Wu B, Li W, Guidon A, Liu C. Whole brain susceptibility mapping using compressed sensing. Magn Reson Med. 2012; 67:137–147. [PubMed: 21671269]

29. Wei H, Dibb R, Zhou Y, et al. Streaking artifact reduction for quantitative susceptibility mapping of sources with large dynamic range. NMR Biomed. 2015; 28:1294–1303. [PubMed: 26313885]

30. Wei H, Zhang Y, Gibbs E, Chen NK, Wang N, Liu C. Joint 2D and 3D phase processing for quantitative susceptibility mapping: application to 2D echo-planar imaging. NMR Biomed. 2016; doi: 10.1002/nbm.3501

31. Feng Y, He T, Gatehouse PD, et al. Improved MRI R2 * relaxometry of iron-loaded liver with noise correction. Magn Reson Med. 2013; 70:1765–1774. [PubMed: 23359410]

32. DeLong ER, DeLong DM, Clarke-Pearson DL. Comparing the areas under two or more correlated receiver operating characteristic curves: a nonparametric approach. Biometrics. 1988; 44:837–845. [PubMed: 3203132]

33. Sharma SD, Hernando D, Horng DE, Reeder SB. Quantitative susceptibility mapping in the abdomen as an imaging biomarker of hepatic iron overload. Magn Reson Med. 2015; 74:673–683. [PubMed: 25199788]

34. Longo R, Ricci C, Masutti F, et al. Fatty infiltration of the liver. Quantification by 1H localized magnetic resonance spectroscopy and comparison with computed tomography. Invest Radiol. 1993; 28:297–302. [PubMed: 8478169]

35. Wood JC. Guidelines for quantifying iron overload. Hematology Am Soc Hematol Educ Program. 2014; 2014:210–215. [PubMed: 25696857]

36. Olivieri NF, Brittenham GM. Iron-chelating therapy and the treatment of thalassemia. Blood. 1997; 89:739–761. [PubMed: 9028304]

37. Harrison SA, Bacon BR. Relation of hemochromatosis with hepatocellular carcinoma: epidemiology, natural history, pathophysiology, screening, treatment, and prevention. Med Clin North Am. 2005; 89:391–409. [PubMed: 15656932]

38. Kang BK, Yu ES, Lee SS, et al. Hepatic fat quantification: a prospective comparison of magnetic resonance spectroscopy and analysis methods for chemical-shift gradient echo magnetic resonance

imaging with histologic assessment as the reference standard. Invest Radiol. 2012; 47:368–375. [PubMed: 22543969]

39. Hong CW, Mamidipalli A, Hooker JC, et al. MRI proton density fat fraction is robust across the biologically plausible range of triglyceride spectra in adults with nonalcoholic steatohepatitis. J Magn Reson Imaging. 2017; doi: 10.1002/jmri.25845

40. Satkunasingham J, Besa C, Bane O, et al. Liver fat quantification: Comparison of dual-echo and triple-echo chemical shift MRI to MR spectroscopy. Eur J Radiol. 2015; 84:1452–1458. [PubMed: 26047820]

41. Zhong X, Nickel MD, Kannengiesser SA, Dale BM, Kiefer B, Bashir MR. Liver fat quantification using a multi-step adaptive fitting approach with multi-echo GRE imaging. Magn Reson Med. 2014; 72:1353–1365. [PubMed: 24323332]

42. Yokoo T, Browning JD. Fat and iron quantification in the liver: past, present, and future. Top Magn Reson Imaging. 2014; 23:73–94. [PubMed: 24690618]

43. St Pierre TG, El-Beshlawy A, Elalfy M, et al. Multicenter validation of spin-density projection-assisted R2-MRI for the noninvasive measurement of liver iron concentration. Magn Reson Med. 2014; 71:2215–2223. [PubMed: 23821350]

44. Xie L, Sparks MA, Li W, et al. Quantitative susceptibility mapping of kidney inflammation and fibrosis in type 1 angiotensin receptor-deficient mice. NMR Biomed. 2013; 26:1853–1863. [PubMed: 24154952]

45. Krafft AJ, Loeffler RB, Song R, et al. Quantitative ultrashort echo time imaging for assessment of massive iron overload at 1.5 and 3 Tesla. Magn Reson Med. 2017; doi: 10.1002/mrm.26592

46. Luo XF, Xie XQ, Cheng S, et al. Dual-Energy CT for Patients Suspected of Having Liver Iron Overload: Can Virtual Iron Content Imaging Accurately Quantify Liver Iron Content? Radiology. 2015; 277:95–103. [PubMed: 25880263]

47. Wang Y, Liu T. Quantitative susceptibility mapping (QSM): Decoding MRI data for a tissue magnetic biomarker. Magn Reson Med. 2015; 73:82–101. [PubMed: 25044035]

48. Henninger B, Kremser C, Rauch S, et al. Evaluation of MR imaging with T1 and T2* mapping for the determination of hepatic iron overload. Eur Radiol. 2012; 22:2478–2486. [PubMed: 22645044]

Key Points

- Magnetic susceptibility showed strong correlation with LIC (r_s=0.918).

- QSM showed high diagnostic performance for LIC, similar to that of R_2^*.

- Simultaneously estimated FF-MRI showed strong correlation with MR-Spectroscopy-based FF (R^2=0.910).

- QSM combining water-fat separation has quantitative value for LIO with coexisted steatosis.
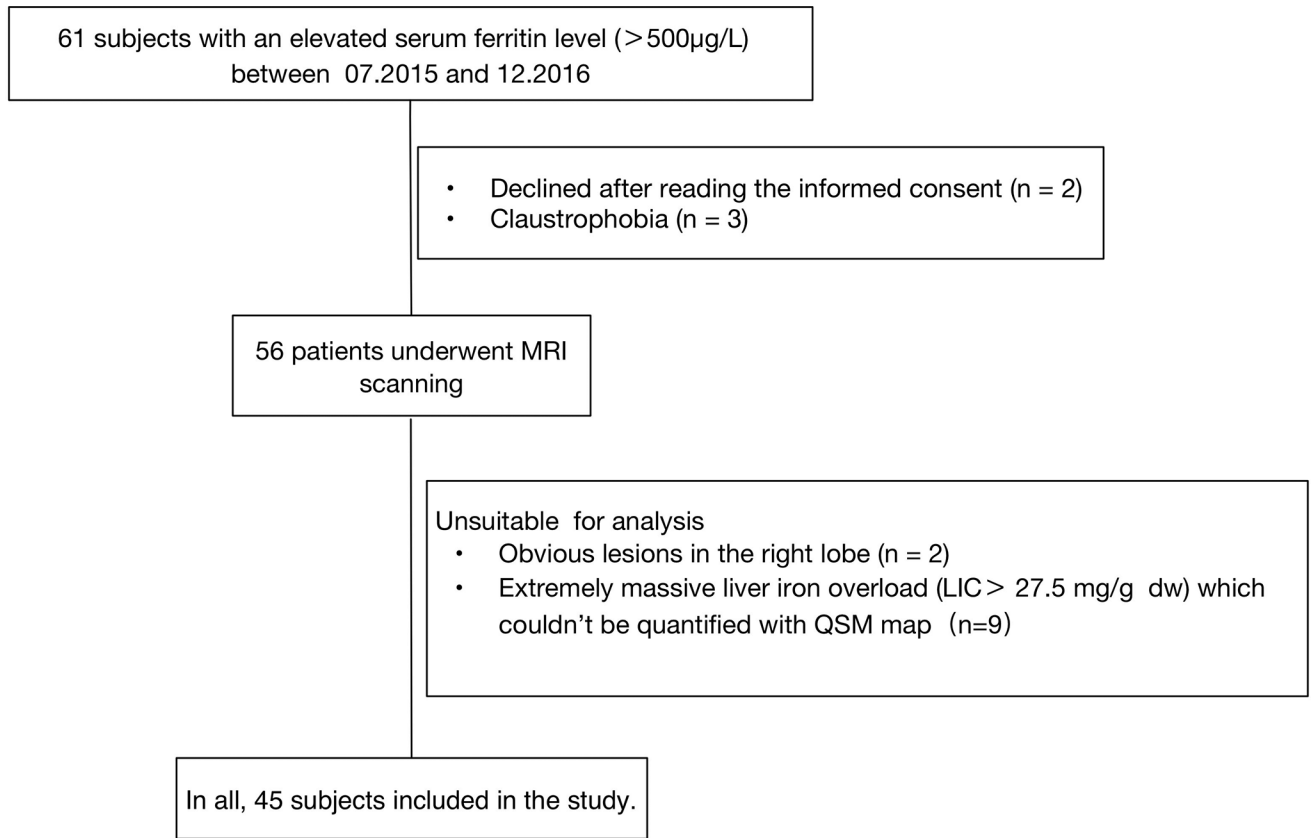
Figure 1.
Flowchart of the patient inclusion process.
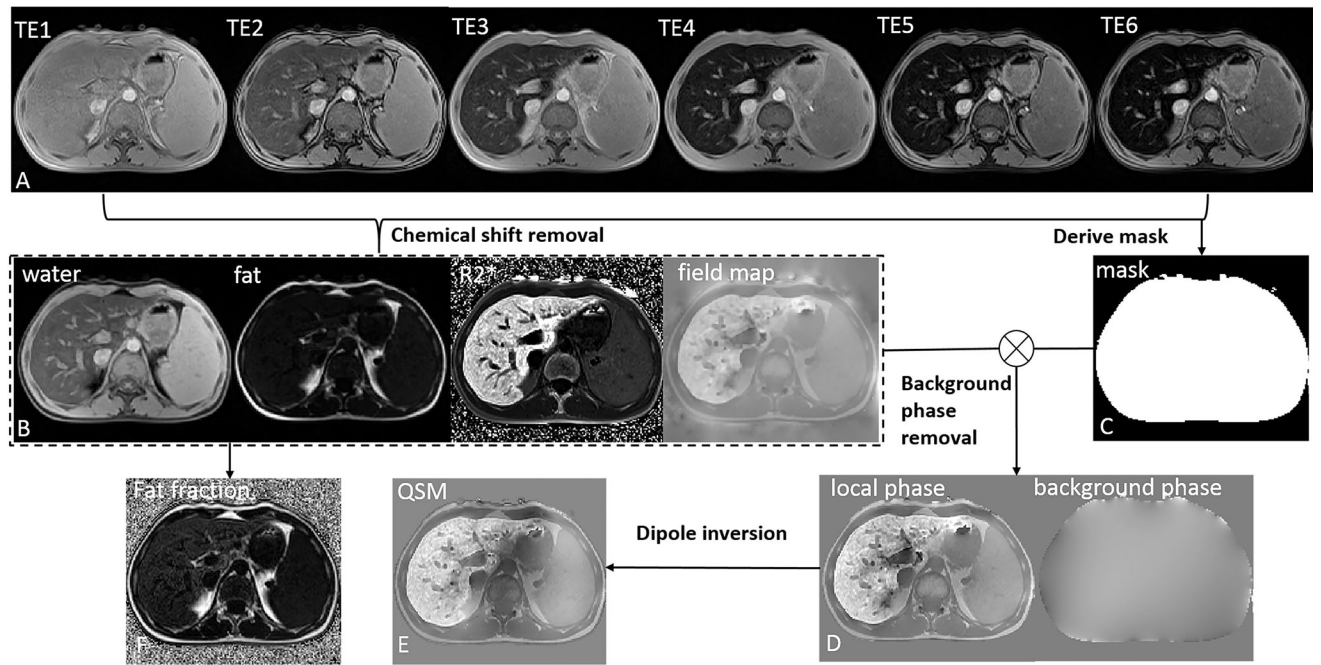
Figure 2.
Processing pipeline to estimate the susceptibility map and fat fraction map of liver. First, complex multi-echo images were used to estimate the B_0 field map, water, fat and R_2^* images (Fig. 2b). Second, the sum-of-squares of the magnitude images were used to obtain a mask (Fig. 2c). This binary mask provided edge information to calculate the local field by removing the background field (Fig. 2d). The local field map is subsequently input to the two-level regularization approach to obtain the QSM maps (Fig. 2e). FF is calculated from estimated water and fat images: FF = fat/ (water + fat) *100% (Fig. 2f).
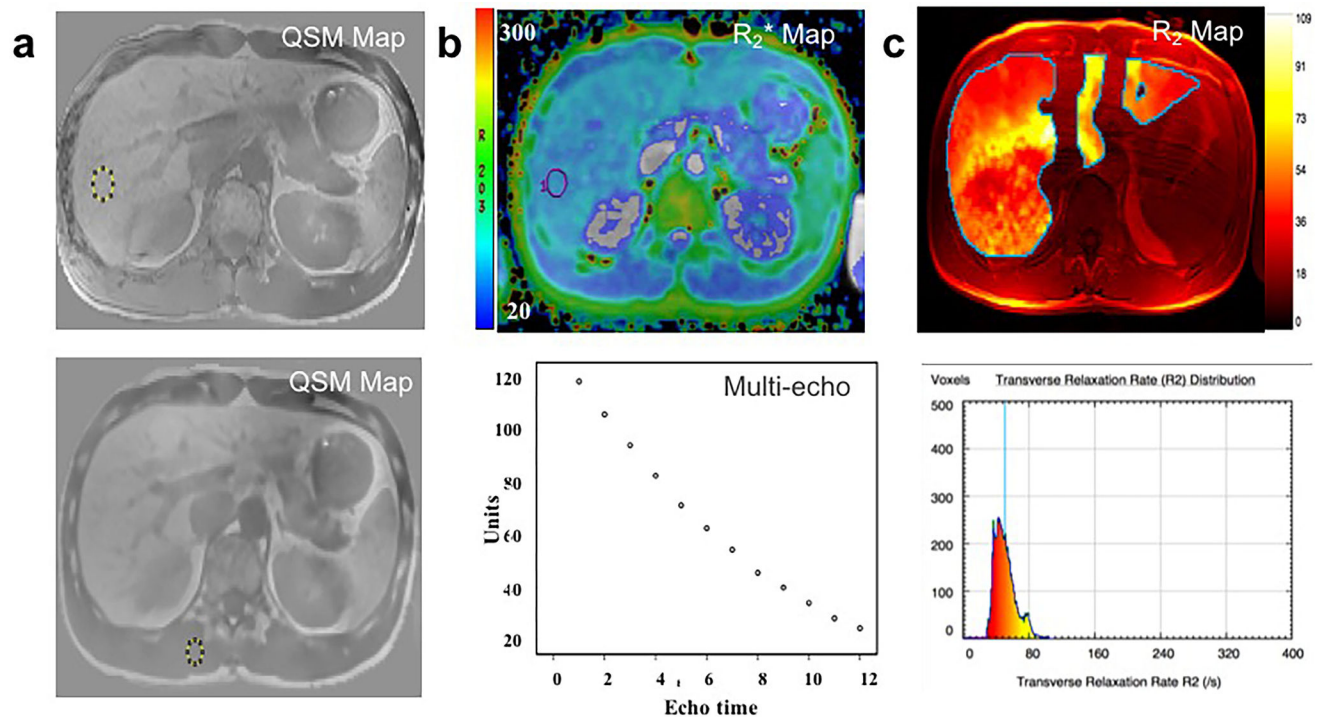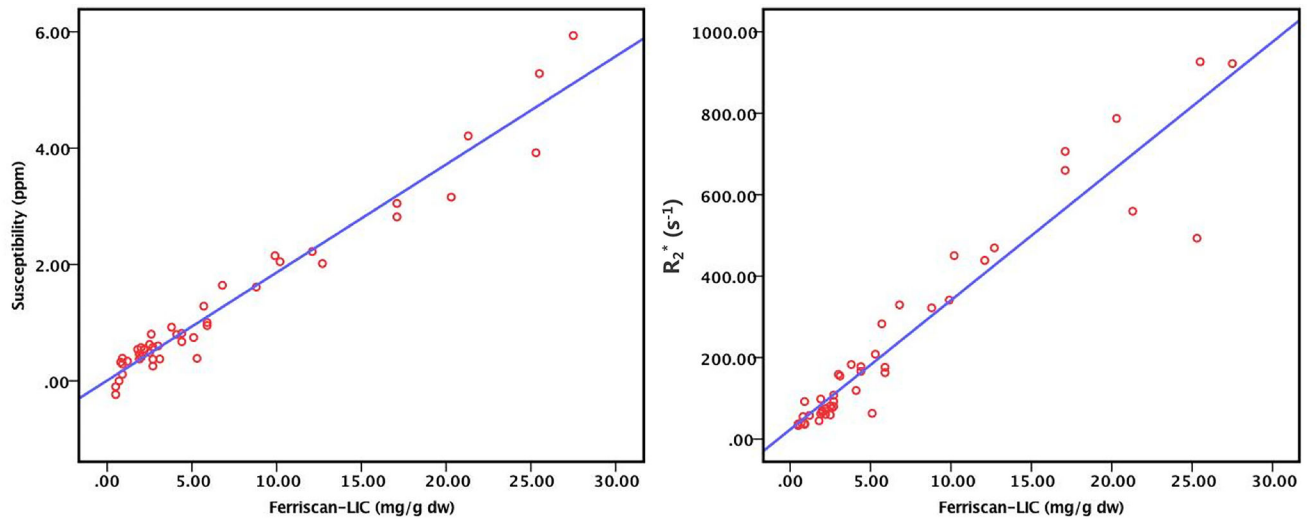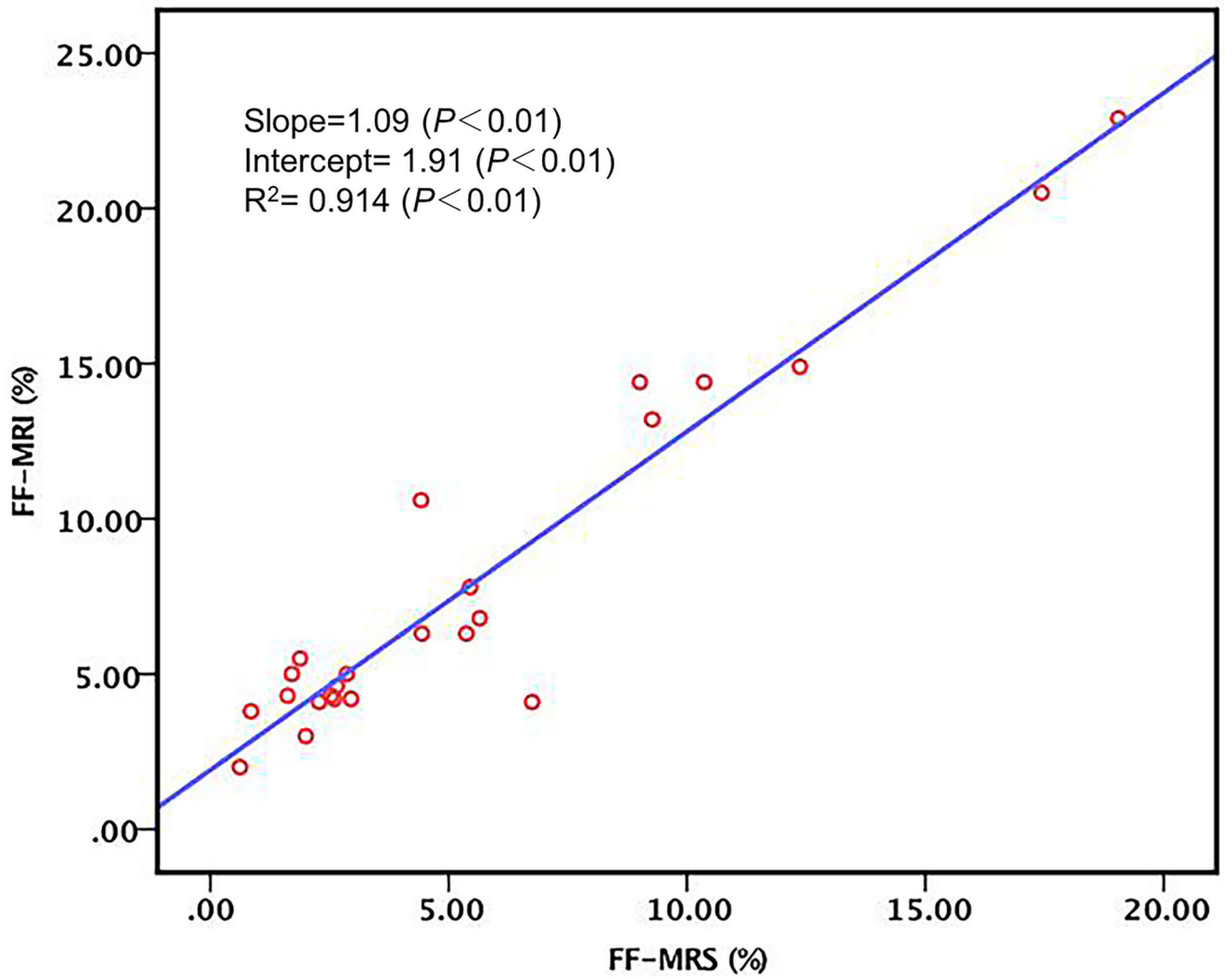
Figure 3.

Susceptibility value, R_2^* and R_2 measurement in a 37-year-old man with elevated Serum Ferritin of unknown aetiology. (a) Top, the liver susceptibility value was measured by placing the circular ROI in segment VI. Bottom, another reference ROI was placed in the paravertebral muscle tissue at the renal hilum level. (b) Top, the ROI of R_2^* was drawn in a visual assignment with that of QSM image in (a). Bottom, signal decays with increasing TE. (c) Top, R_2 map shows that large vascular structures and other image artefacts were excluded from the analysis of R_2 map. Bottom, the R_2 histogram illustrates the R_2 estimation of 51.1 ± 12.2 s^{-1}. The LIC was 2.0 mg/g dw (normal range, 0.17~1.8 mg iron per gram dry tissue).
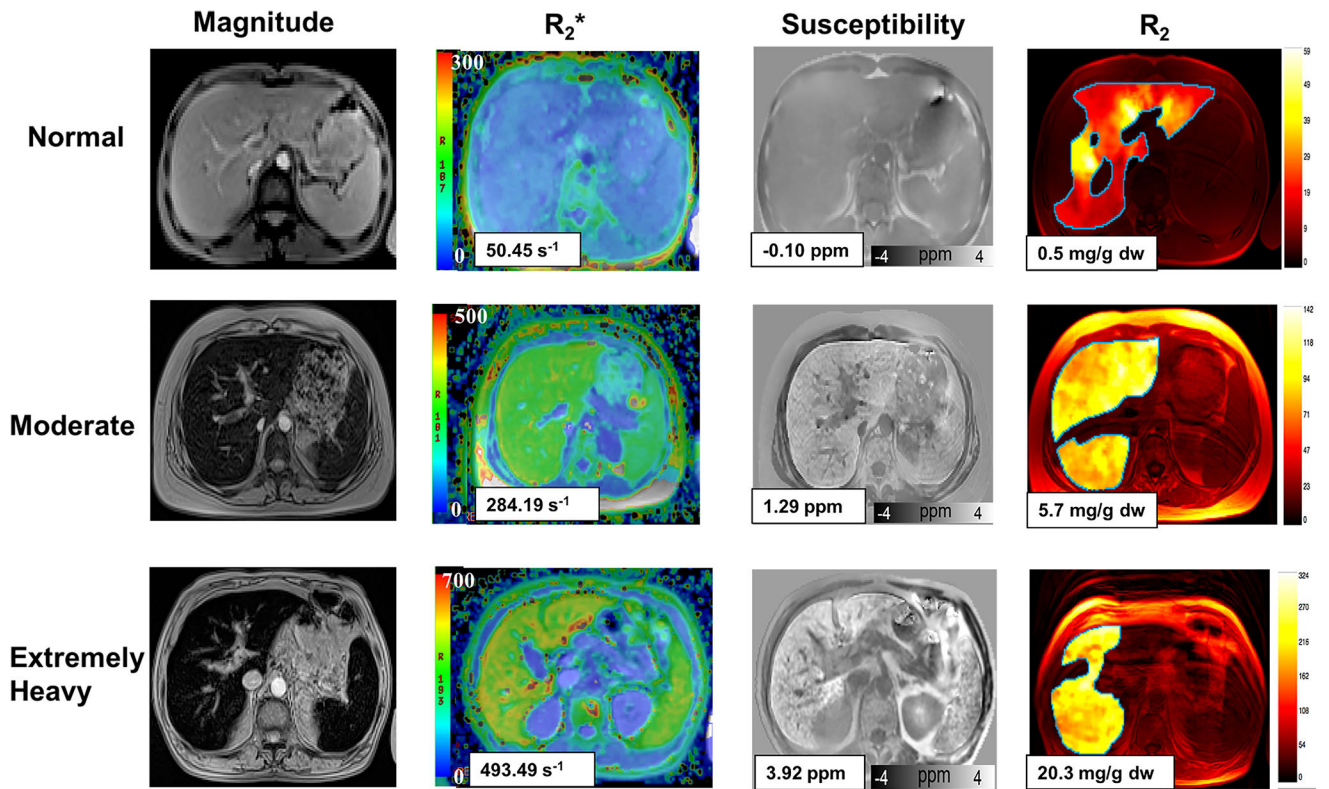
Figure 4.
Magnitude (original VIBE images at TE=8.24 ms), R_2^*, QSM maps and FerriScan-R_2 for three subjects, including 18-year-old man with leukaemia, 18-year-old woman with aplastic anaemia, and 59-year-old woman with aplastic anaemia.

Figure 5.

Scatterplot shows a positive correlation between QSM and FerriScan-LIC, and between R_2^* and FerriScan-LIC (r_s=0.918, P<.001; r_s=0.946, P<.001, respectively).45 patients were included for the estimation of QSM and R_2^*.

Figure 6.
Correlation between FF-MRI and FF-MRS for 24 patients (R^2=0.910, P<.001).

Table 1

Summary of Demographic and Clinical Characteristics

Parameter	Value	Parameter	Value
Demographic characteristics		**Clinical characteristics**	
No. of patients	45	Myelodysplastic syndrome	11
Sex		Aplastic anemia	9
No. of men	31	Chronic liver disease	5
No. of women	14	Thalassemia	3
Mean age(y) [*]		Hemochromatosis	2
All patients	44.36 (18~73)	leukemia	2
		pancytopenia	1
Men	44.45 (18~71)	Unknown	12
		Serum ferritin level (ng/ml)	
Women	44.14 (18~73)	Mean ± SD [†]	1337.65±717.35
		Range	512.8~3947.4

[*] Numbers in parentheses are ranges;

[†] SD=standard deviation.

Table 2

Acquisition Parameters for Sequences

Sequence	TE₁ (ms)	Echo spacing	Number of echoes	TR (ms)	Flip angle (deg)	Bandwidth (Hz/pixel)	FOV (mm²)	Matrix size	Slice thickness (mm)	Number of slice
3D VIBE	1.44	1.36	6	10	6	1040	420×315	224×168	5	44
2DGRE (fat-saturated)	1.09	1.56	12	50	20	1500	400×275	128×88	10	10
2D FerriScan	6	3	5	1000	90	500	400×300	256×192	5	11

Comparison of LIC Grading Performance with QSM and R_2^*.

Table 3

LIC Threshold (mg/g dw)	Susceptibility value (ppm)				R_2^* (s^{-1})				Z Value	P Value
	Optimal cutoff(ppm)	Sensitivity	Specificity	AUC	Optimal cutoff (s^{-1})	Sensitivity	Specificity	AUC		
1.8	0.34	0.97 [35/36] (0.86,0.99)	0.78 [7/9] (0.4,0.97)	0.948 (0.837,0.992)	58.01	1 [36/36] (0.93,1)	0.89 [8/9] (0.52,1)	0.969 (0.869,0.998)	0.57	0.57
3.2	0.63	0.96 [21/22] (0.77,1)	0.96 [22/23] (0.78,1)	0.970 (0.871,0.998)	158.86	0.91 [19/21] (0.71,0.99)	1 [23/23] (0.85,1)	0.972 (0.874,0.999)	0.06	0.95
7	1.29	1 [12/12] (0.735,1)	0.97 [32/33] (0.84,1)	1 (0.916,1)	282.94	1 [12/12] (0.74,1)	0.97 [32/33] (0.84,1)	0.997 (0.916,1)	0	1
15	2.22	1 [7/7] (0.59,1)	1 [38/38] (0.91,1)	1 (0.921,1)	469.31	1 [7/7] (0.59,1)	1 [38/38] (0.91,1)	1 (0.921,1)	0	1

Note: Numbers in brackets are raw data. Numbers in parentheses are 95% confidence intervals. FerriScan-LIC was used as the standard of reference.